Submitted to Perception. Revised Dec. 2002

Motion, flash and flicker: a unified spatio-temporal model of perceived edge sharpening

Stephen T. Hammett[#]

Mark A. Georgeson §

Gillian S. Barbieri-Hesse §

[#] Department of Psychology
Royal Holloway College
University of London
Egham Surrey TW20 0EX UK

e-mail: s.hammett@rhul.ac.uk or steve@castor.pc.rhul.ac.uk
tel: +44 1784 443702
fax: +44 1784 443702

§ Neurosciences Research Institute
Aston University
Birmingham B4 7ET UK
e-mail: m.a.georgeson@aston.ac.uk

Abstract

Blurred edges appear sharper in motion than when they are stationary. We (Hammett, Georgeson & Gorea, 1998) proposed a model of this motion sharpening that invokes a local, non-linear contrast transducer function. Response saturation in the transducer compresses or 'clips' the input spatial waveform, rendering the edges as sharper. To explain the increasing distortion of drifting edges at higher speeds, the degree of nonlinearity must increase with speed or temporal frequency. A dynamic contrast gain control before the transducer can account for both the speed dependence and approximate contrast invariance of motion sharpening (Hammett et al, 2003, in press). We show here that this model also predicts perceived sharpening of briefly flashed and flickering edges, and we show that the model can account fairly well for experimental data from all three modes of presentation (motion, flash and flicker). At moderate durations and lower temporal frequencies the gain control attenuates the input signal, thus protecting it from later compression by the transducer. The gain control is somewhat sluggish, and so it suffers both a slow onset, and loss of power at high temporal frequencies. Consequently brief presentations and high temporal frequencies of drift and flicker are less protected from distortion, and show greater perceptual sharpening.

Introduction

The fact of temporal integration in vision (eg. Barlow, 1958; Legge, 1978; Gorea & Tyler, 1986; Georgeson, 1987) leads one to expect that moving objects should appear more blurred than stationary ones. There is much psychophysical evidence for the existence of such motion blur (e.g. Burr, 1980; Pääkkönen & Morgan, 1994; Chen, Bedell & Ogmen, 1995). However, blurred edges in motion appear sharper than their static analogues, rather than appearing even more blurred (Ramachandran et al, 1974; Bex, Edgar & Smith, 1994; Hammett & Bex, 1996, Hammett, 1997; Hammett, Georgeson & Gorea, 1998). It has also been observed that briefly flashed edges look sharper, even without motion (Galvin et al, 1999; Georgeson & Hammett, 2002). Our aims in this paper are to test whether a third form of temporal modulation – counterphase flicker – also produces edge sharpening, and then to devise a plausible, dynamic computational model that may unify the results from these three types of experiment.

A variety of explanations has been proposed to account for motion sharpening. One possibility is that the visual system invokes some 'default' assumption that edges in motion are sharp (e.g. Burr & Morgan, 1997). Temporal integration renders high spatial frequencies undetectable at fast speeds and so sharp and blurred edges will be indistinguishable; the system might then pre-suppose that edges are sharp when there is no information to the contrary. Hammett & Bex (1996) tested this possibility using an adaptation protocol. They reasoned that if sharpening was due to a default assumption of sharpness then reducing the sensitivity of the visual system to high spatial frequencies should have no effect (or possibly increase) motion sharpening. They found that adaptation to high spatial frequencies (a missing-fundamental square-wave grating) reduced

the magnitude of the motion sharpening effect. Thus the results of adaptation experiments do not support a 'default' model of sharpening.

An alternative explanation is that motion blur is compensated by the visual system (Anderson & Van Essen, 1987; Martin & Marshall, 1993). This type of explanation invokes a scheme whereby information about the speed of the edge is used to compensate for motion induced blur. However, whilst these models may explain the relative lack of motion blur experienced by observers (e.g. Burr, 1980), they do not predict a *sharpening* of moving edges. Nor do they provide an explanation for the perceived sharpening of briefly flashed edges that are not moving (Galvin et al, 1999; Georgeson & Hammett, 2002).

More recently Pääkkönen and Morgan (2001) have shown that a bi-phasic temporal impulse response of the visual system can, in principle, account for both motion blur and motion sharpening. However, because the model is linear it cannot account for the motion sharpening observed for pure sinusoidal gratings (e.g. Bex et al, 1995, Hammett & Bex, 1996), and because it depends on motion it cannot account for the sharpening of stationary, flashed edges.

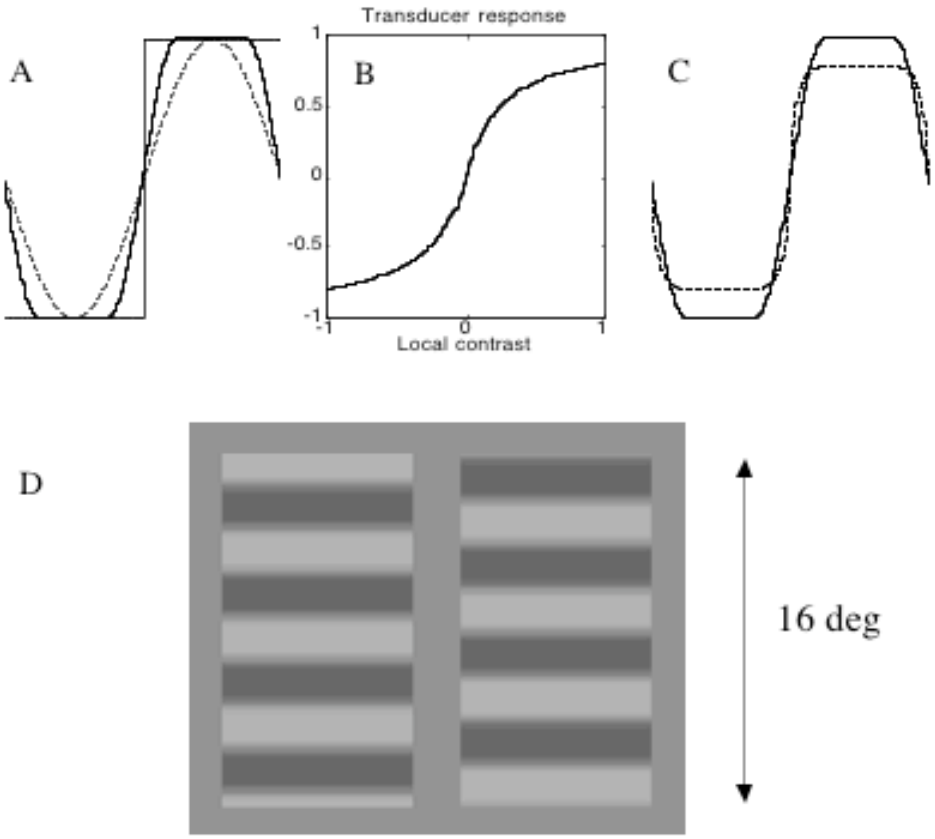

Fig 1. A: the range of variation in luminance profiles of stimuli from square-wave to sinusoid. The solid curve is a blur profile constructed by replacing the square-wave edges with sine-wave half-periods centred on the edges. Edge blur width is defined by this half-period, in min arc. B: Example of the sigmoidal transducer function defined by equation 1. C: How a blurred grating (solid curve) is sharpened (dashed curve) by the transducer shown in (B). D: layout of the two stimulus windows on the display screen; shown to scale for an edge width of 60 min arc (spatial frequency, 0.25 c/deg).

In short, we still lack a general explanation that is not defeated by one or other variant of the sharpening phenomenon. We offered an account of motion sharpening that assumes an early, speed-dependent non-linearity (Hammett, Georgeson & Gorea, 1998). The model proposed that distortions in edge encoding are mediated by a non-linearity in the contrast response function

(Fig. 1B). In this model, the spatial response profile R(x) of the transducer output is a function of the local contrast C(x) of the input image:

$$R(x) = \frac{Cx)}{S + |C(x)|}, \qquad (1)$$

where $C(x) = (L(x)-L_0)/L_0$, L(x) is the luminance profile and L_0 is mean luminance. The saturation constant (S) controls the compressiveness of the transducer, and smaller values make it more compressive. The compressive contrast response function leads to a sharpening of blurred edge waveforms (Fig. 1C).

This idea offers a basis for motion sharpening but does not account for the near contrast-invariance that we reported recently (Hammett et al, 2003), nor does it explain why or how the transducer becomes more compressive with increasing speed. To account for these factors, we extended the transducer model to incorporate a contrast gain control that precedes the transducer (Fig. 2). The model is fully described in another paper (Hammett et al, 2003) and so we only summarize it here; model equations are given in the Appendix. The gain control (Fig. 2) uses a pair of spatially even- and odd-symmetric filters to evaluate the contrast energy (R2) in the input image, averaged across a neighbourhood in space and time. The gain control signal G, a simple linear function of R2, is then used to scale down the image signal amplitude (R1) before input to a static, compressive transducer. The broad purpose of the gain control would be to exploit the dynamic range of the transducer, but to prevent saturation of high contrast signals. Because the filter f2 integrates across time, the filter responses R2 and the subsequent gain control signal (G) are attenuated at high temporal frequencies. This in turn means that the scaled signal amplitude (R3 = R1/G) – input to the transducer – is higher, and so suffers more compression and more sharpening, at faster speeds where G is lower.

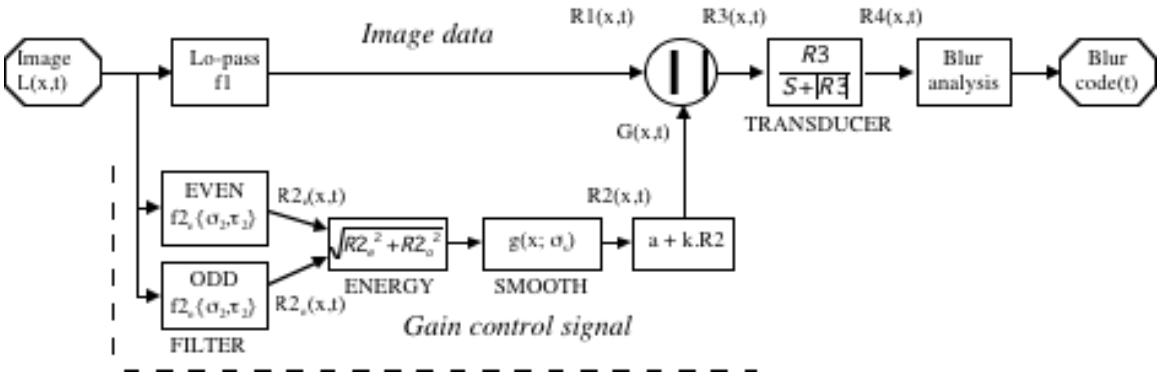

Fig 2. Block diagram of the transducer model, with dynamic contrast gain control (Hammett et al, 2003).

By this qualitative argument, we might also expect the same logic to hold for fast flicker as well as fast movement. That is, flickering (counterphase) edges might look sharper at higher flicker rates. The purpose of this paper is to test experimentally whether this is so, and to establish whether the model (Fig. 2) can account for the observed effects of flicker and motion. We have also found that briefly presented edges appear sharper than edges presented for longer durations (Georgeson & Hammett, 2002), and so a third aim is to challenge the model further with these data on flashed edges, in search of a unified explanation.

Method

Apparatus and Stimuli

Achromatic (greyscale) grating patterns were generated by a VSG2/3W (Cambridge Research Systems) graphics board with 14 bit resolution, and displayed on an Eizo 6600M greyscale monitor at a frame rate of 120 Hz. The mean luminance was 31 cd m^{-2}. The display was gamma corrected (linearized) using internal look-up tables. The stimuli were displayed in two windows, equidistant from a central dark fixation point. The windows subtended 16 degrees (vertical) by 8 degrees (horizontal) and were separated horizontally by 2 degrees. The viewing distance was 57 cm.

The stimuli were horizontal periodic gratings whose luminance profile could vary between sine-wave and square-wave while the spatial period was held constant. To control the degree of blur, each edge of a square wave was replaced by half a cycle of a sine-wave centred on the edge (see Fig. 1A and Bex et al, 1995). Blur width was defined as the half-period of this sinusoidal profile, in min arc. Variations in blur width did not change the fundamental spatial frequency of the grating.

The stimuli flickered (sinusoidal counterphase modulation of contrast) at a range of temporal frequencies (0 - 16 Hz). The peak Michelson contrast of the patterns was always 0.3.

Procedure

Standard and test patterns of the same spatial frequency were presented simultaneously in the two windows, and the left or right position of the two patterns was randomised from trial to trial. The patterns were presented for 500 ms with abrupt onset and offset. Between presentations, a homogeneous grey field of mean luminance was presented. The spatial phase of the standard and test patterns was randomised from presentation to presentation. The standard pattern was a flickering blurred square wave (0.25, 0.5 or 1 c/deg) whose edge blur width (60, 30 or 15 min arc respectively) was constant in any session. At the beginning of each session the blur width of the stationary test pattern was randomised such that it was within +/-20% of the standard pattern. The blur width of the test pattern subsequently varied from trial to trial depending upon the subject's previous responses. Its blur width was determined by a modified Pest procedure (Taylor and Creelman, 1967) set to converge on the 50% point of subjective equality (PSE). The subjects' task was to indicate which of the two patterns appeared sharper by pressing a button. The test pattern was static and the standard pattern flickered at 0, 2, 4, 8 or 12 Hz. The "spatial

frequency doubling" phenomenon (Kelly 1966, 1981) occurs at lower spatial and higher temporal frequencies, and can make the task of judging edge blur difficult and ambiguous. Thus the highest flicker rate at which meaningful data could be collected was restricted to 12 Hz (1 c/deg), 8 Hz (0.5 c/deg) or 4 Hz (0.25 c/deg). Each session consisted of 40 trials for each temporal frequency. The 50% point of the resultant psychometric function was estimated by Probit analysis (Finney, 1971). The PSE was taken to be the mean of four such estimates. The order of sessions was pseudo-random.

In order to compare the effect of flicker and motion on perceived edge blur we conducted an auxiliary experiment that measured perceived sharpness for drifting stimuli. The experiment was similar to that described above except that the stimuli drifted instead of flickering. The range of temporal frequencies tested was similar to the flicker experiment. The direction of drift (up or down) was randomised from trial to trial. In all other respects, the procedure was as described above.

Two subjects participated in the experiment, S.B. who was aware of the general purpose of the experiment, and a naive but well practised observer (D.S.). Viewing was binocular and no head restraint was used. The experiment was conducted in a semi-darkened room.

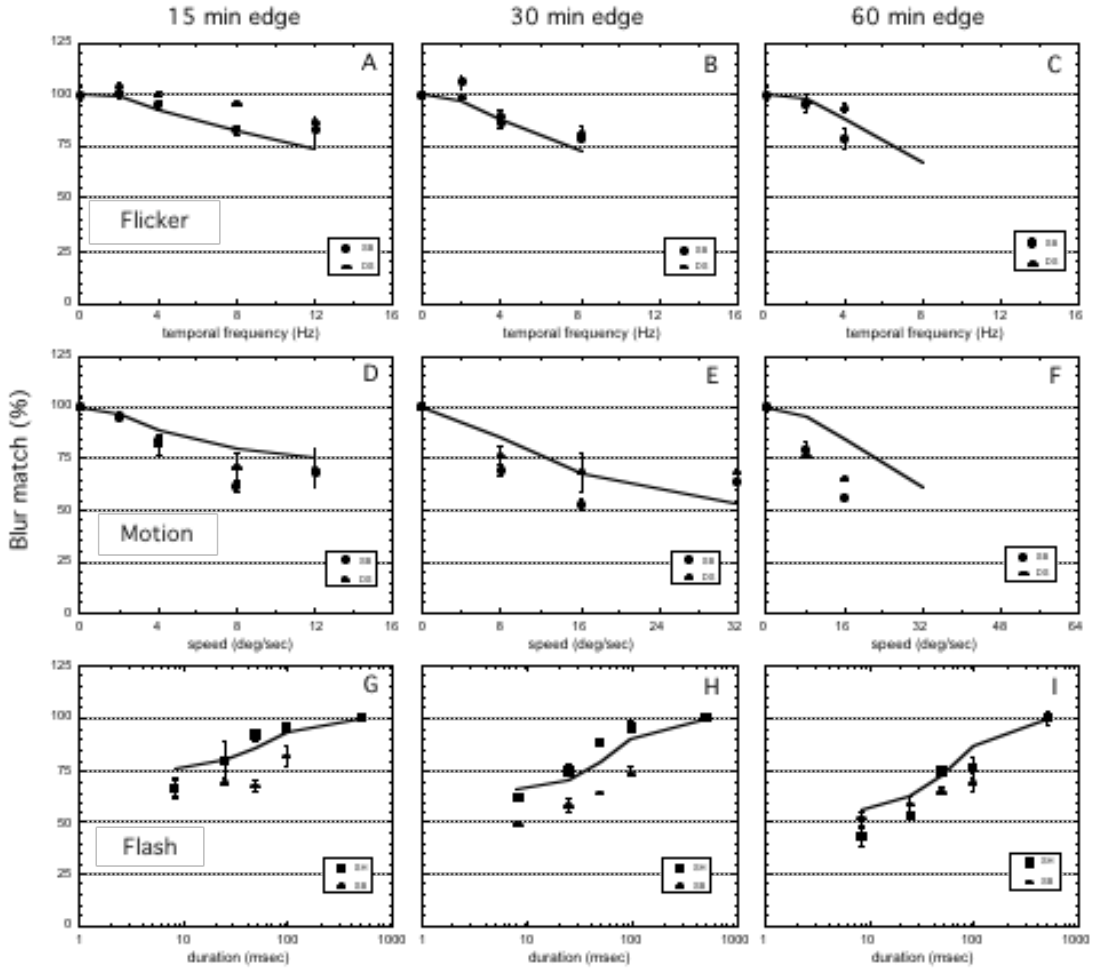

Fig 3. Blur matching results for two observers (different symbols ± 1 s.e.) for flickering (A,B,C), moving (D,E,F) and flashed (G,H,I) edges. Edge widths were 15, 30, and 60 min arc, as shown for each column. For the motion graphs (D,E,F) both the speed axis (below) and the temporal frequency axis (above) are appropriately scaled. Solid curves show predictions of the gain control model using parameters given in the appendix. Experimental blur matches (and model blur codes) are expressed as percentages of the baseline match (or code). Data in G,H,I are re-plotted from Georgeson & Hammett (2002) for the same edge widths (15, 30, 60 min) as above, but in this case the gratings were pure sine-waves without the luminance plateau shown in Fig. 1A.

Results

Psychophysics

Fig 3 (top two rows) shows the results for the two observers for both flickering and moving stimuli. For each speed or temporal frequency, mean blur match (B) for a given observer was expressed as a percentage (P) of the baseline blur match (B_0) made at 0 Hz or 0 deg/sec: P = $100*B/B_0$. Thus in fig. 3 matches below 100% represent perceived sharpening of edges.

Sharpening was clearly observed for flickering stimuli (Fig. 3A,B,C) and it increased with temporal frequency, but the sharpening effect was consistently greater for moving stimuli (Fig. 3D,E,F) at corresponding temporal frequencies. The percentage sharpening can be expressed as (100-P), and these values are plotted in Fig. 4, to compare the sharpening for flicker and for motion at corresponding temporal frequencies. Flicker sharpening was around half, or less than half, the motion sharpening observed at the same temporal frequency.

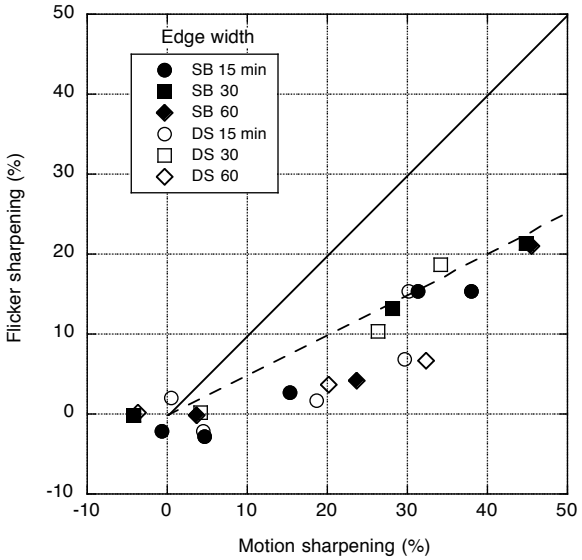

Fig 4. Data re-plotted from Fig. 3 A,B to compare the percentage sharpening induced by motion and by flicker at corresponding temporal frequencies for observers SB (filled symbols) and DS (open symbols). Lines of slope 1 (solid) and 0.5 (dashed) are shown.

Modelling

How well can the model of Fig. 2, with a dynamic contrast gain control followed by a static, compressive transducer, account for these results? Model predictions were derived for the spatiotemporal stimuli used here, and by Georgeson & Hammett (2002). For each stimulus the final edge blur code produced by the model was expressed as a percentage of the baseline code, as was done with the experimental blur matches. Solid curves in Fig. 3 show the predictions of the model with parameter values given in Table 1. Overall, the model captures the phenomena fairly well. The magnitude of flicker sharpening, and its temporal dependence (Fig 3A,B,C) are well described. For motion sharpening (Fig 3D,E,F), the model fit with these parameters was not

quite so good. Although the trend with increasing speed was fairly well described, the model did not predict the greater sharpening observed for motion than for flicker, especially with the 60 min edge width (Fig. 3F).

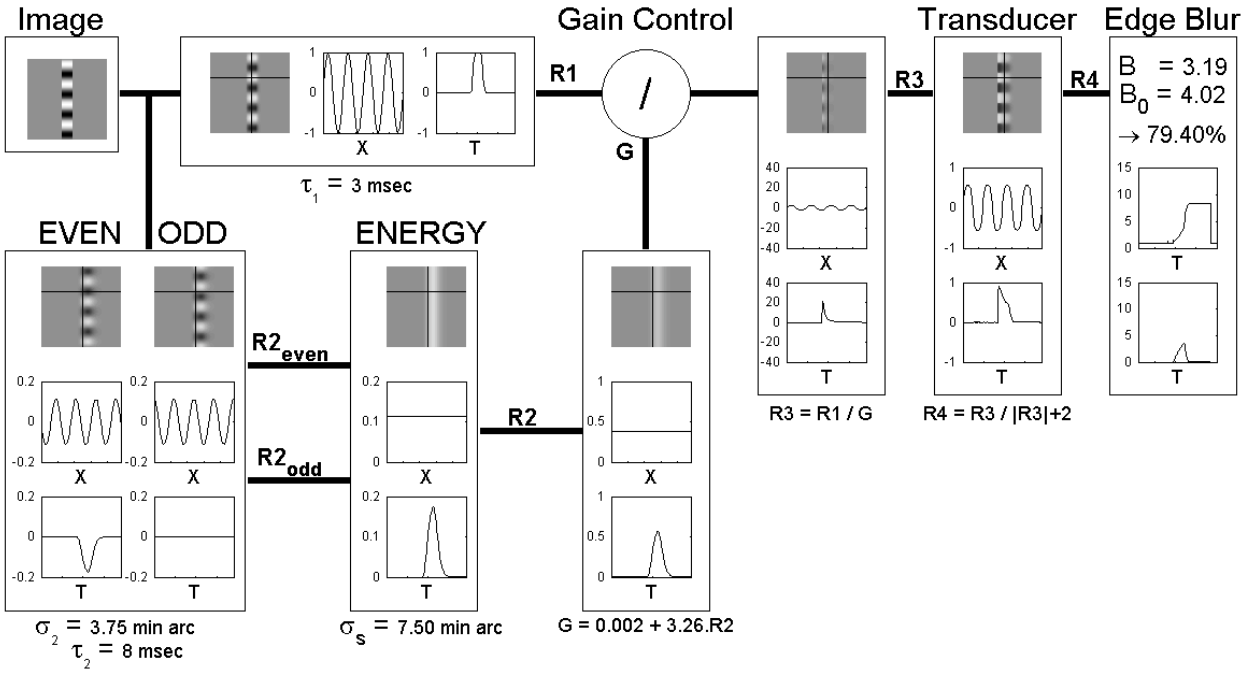

Fig 5. Worked example of the gain control model (Fig. 2) for a 48 ms flashed grating with edge width = 30' (period 60'). Model parameters given in Table 1. Each pane shows a space-time image of the response at a given stage (horizontal axis is time), along with graphs of spatial (X) and temporal (T) profiles taken at the positions marked by black lines in the space-time image. X-range is 240 min arc, T-range is 375 ms. Large early spike in the response R3 reflects delay in the gain control signal (where G is briefly low) but because of saturation this spike is not so prominent in the transduced signal, R4. Final coding of edge blur operates on the R4 signal, as described in the text. Final pane (right) shows the raw blur code b(t) (upper graph) and the contrast-weighted blur code b(t).w(t)/max(w) (lower graph). The final blur estimate B is the weighted average of b(t), and is compared with the baseline estimate (B_0) obtained from a 500 ms presentation. This percentage (79%) implies that 21% sharpening is predicted for this stimulus condition.

Importantly, however, the model did give a good account of the sharpening observed for flashed gratings (Fig. 3G,H,I). These data represent the perceived blur of edges that were shown for durations of 8 to 500 ms and matched by a standard edge shown for 500 ms, re-plotted from Georgeson & Hammett (2002). The edge widths chosen for re-analysis were the same as tested here (15, 30, 60 min), but the gratings were pure sine-waves without the luminance plateau shown in Fig. 1A. In all cases we simulated the space-time images appropriate for each

experiment. The magnitude of sharpening and the trend for greater sharpening at shorter durations are well described by the model.

Why does the model predict edge sharpening for flashed and flickering gratings? Figs. 5-7 give some insight by illustrating the space-time distributions of response at each stage of processing. We begin with the simpler example of a sine-wave grating flashed for 48 ms (Fig. 5). The even and odd spatial filters give sine- and cosine-phase responses respectively, and so the energy image is spatially uniform [because $\sin^2() + \cos^2() = 1$]. The energy (R2) rises and falls with flash onset and offset, but is smoothed and delayed by the low-pass temporal filtering action of f2. This delay is crucial to understanding the effect of duration. For a short time, the image signal (R3) passes to the transducer at high amplitude before the gain signal G has had time to damp it down, and so it suffers strong compression and sharpening. Notice how the blur code (fig 5, right, upper graph) begins at a low (sharp) value but then rises as G takes control. Our model supposes that the final blur code *B* is a weighted average of the blur codes *b(t)* evoked over time, and we used the magnitude |R1(t)| as a suitable set of weights w(t). It is reasonable that values of b(t) should contribute little to the final blur estimate B at times when stimulus contrast is near zero, and since the weights w(t) closely follow the temporal envelope of stimulus contrast they achieve that goal. Note how a large plateau in the raw blur code (fig 5, right, upper graph) disppears when the weights are applied (fig 5, right, lower graph). Hence the final blur code is given by:

$$B = \frac{\sum w(t).b(t)}{\sum w(t)}.$$

B is sharper when duration is short, but gradually returns towards a larger (more veridical) value at longer durations as the early sharpening is outweighed by later, larger values of blur *b(t)*. Clearly the magnitude of sharpening and the way it varies with duration will depend critically on the interaction of several factors, determined by the choice of parameter values for the gain

control and the transducer. We chose values (see Appendix) that gave a good fit overall to the data of Fig. 3, and differed in only one notable respect from those of Hammett et al (2003) (namely, reduction of τ_2, see Appendix for a justification). We emphasize that it is far from trivial that a good fit is possible at all.

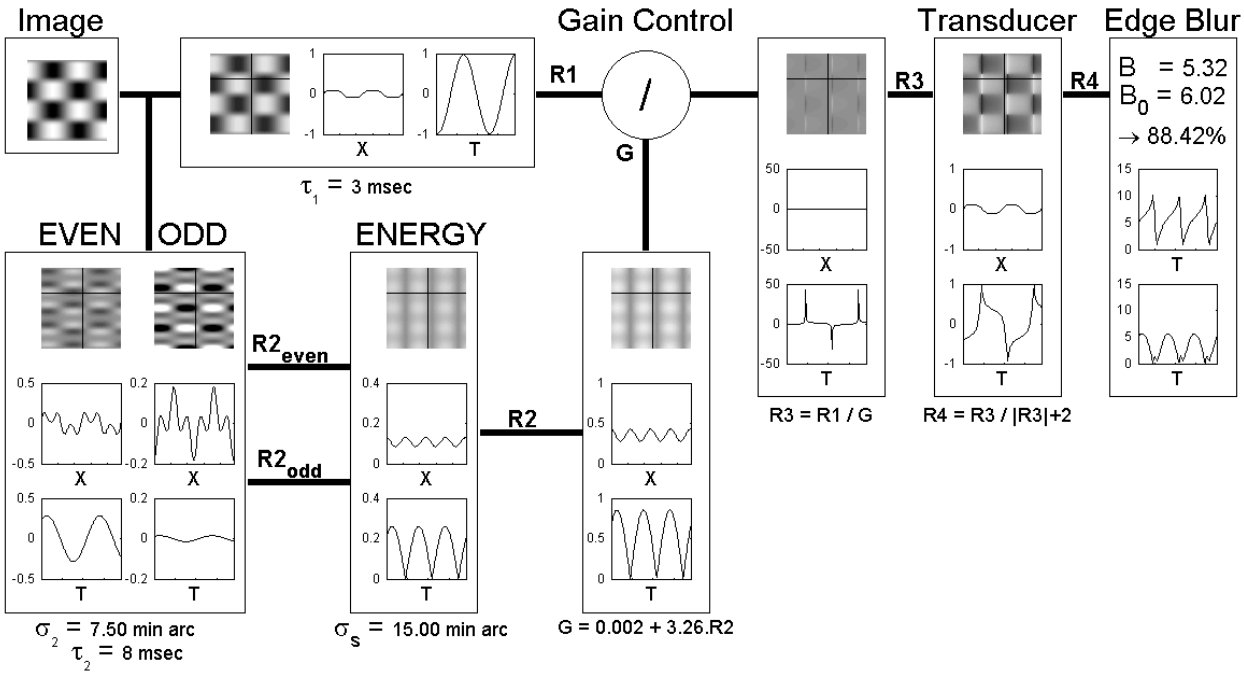

Fig 6. Similar to Fig. 5, but for 4 Hz counterphase flicker, with edge width = 30' (period 120').

Figs. 6 and 7 illustrate in a similar way the model responses to counterphase flicker at 4 Hz and 8 Hz. Because the grating is not a pure sine-wave, the bandpass spatial filter responses are more complex, showing a strong response to the first and third spatial harmonics. Following spatial smoothing, the energy image R2 still shows some spatial modulation, and 100% temporal modulation driven by the counterphase flicker. Thus the gain G modulates strongly at 8 or 16 Hz (ie. twice the flicker rate). The gain modulation and contrast modulation interact to determine the moment-by-moment amplitude of input (R3) to the transducer, and the consequent variation in blur code b(t). In these two examples, the latter has an almost sawtooth variation at 8 or 16 Hz. The extremes of this variation, however, receive little weight because they occur at times when

contrast [and hence the weights w(t)] are low (Figs. 6 and 7, right pane, lower graph). After the weighted averaging the net effect at 4 Hz (Fig. 6) is a modest (12%) sharpening of the final code B, in comparison with the baseline (0Hz) code B_0, as plotted in fig 3B. At 8 Hz, the peak gain G is further attenuated and the net sharpening effect is larger – around 28% (Fig. 7).

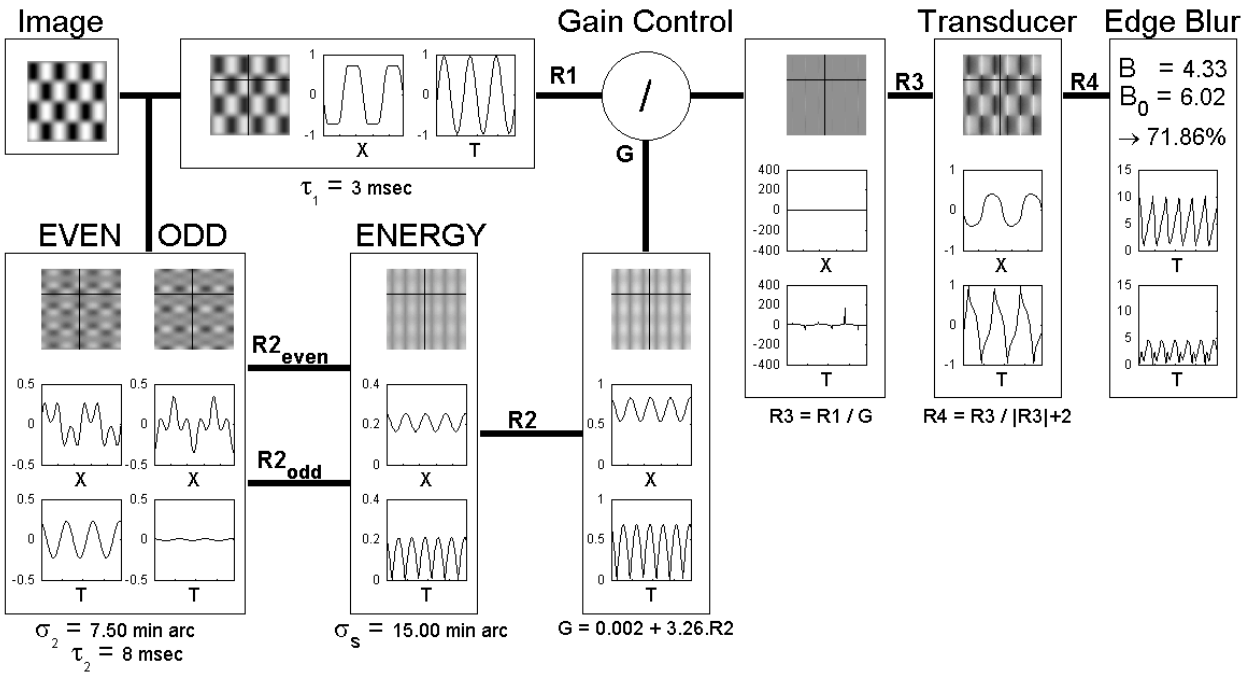

Fig 7. Similar to Fig. 6, but for 8 Hz counterphase flicker, again with edge width = 30' (period 120').

Discussion

This study has shown that flickering blurred edges do appear sharper than stationary ones, and that the sharpening effect for flicker is smaller than for moving edges (Fig. 4). A model consisting of a static, compressive, local contrast response function, preceded by a dynamic, divisive gain control with a somewhat sluggish temporal response gives a good overall account of the sharpening effects for flash, flicker and motion (Fig. 3). The model also predicts contrast-invariant sharpening, as reported in detail by Hammett et al (2003). In its present form the model was not able to capture the greater effect for motion compared with flicker. Nevertheless, its overall success gives us a useful framework for understanding these dynamic distortions of edge

coding. By contrast, no previous proposal (see Introduction) comes close to accounting for the effects of flash, flicker and motion, for sine-wave and non-sine-wave profiles, at a wide range of contrasts, blurs, temporal frequencies and durations.

Although it is conceptually quite simple, the model implies that the spatial and dynamic effects underlying sharpening can be quite elaborate. The quantitative predictions depend not only on the gain control parameters but also upon the model adopted for blur coding, and the manner in which the time-varying blur code is aggregated to return a single judgement of blur. We adopted a parameter-free model for blur that has proved very successful on a wide variety of stationary images (Georgeson, 2001; Barbieri-Hesse & Georgeson, 2002), and we chose a very simple form of weighted averaging to derive the final blur estimate.

Neural basis

The psychophysical experiments give no direct evidence about the possible site(s) for these processes in the visual nervous system, but our best guess is that the gain control and transducer mechanisms are retinal, while the multi-scale blur coding process is cortical. Studies of Y cells in the cat retina (eg. Shapley & Victor, 1978, 1979) and M-cells in the primate retina (Benardete & Kaplan, 1999) have revealed that, for stimulus temporal frequencies up to about 16 Hz, response gain is scaled down markedly with increasing contrast – an effect attributed to the presence of a dynamic contrast gain control mechanism in the retina. M-cells are subject to this gain control, but P-cells appear not to be (Benardete, Kaplan & Knight, 1992). Accounts of contrast gain control in the retina have often been expressed as feedback networks (eg. Shapley & Victor, 1981; Berry et al, 1999), but for simplicity and stability we used a feed-forward control signal in our model. The structure of our model was partly inspired by the work of Wilson (1997) who

constructed a broader and more complex account of retinal function but which includes a divisive gain control prior to a saturating nonlinearity at the ganglion cell level. Thus it is tempting to assign our gain control and transducer to the retina, but we should be cautious. The increasing weight of evidence for additional gain controls at multiple cortical sites (eg. V1 and MT; see Heeger, 1992; Simoncelli & Heeger, 1998; Schwartz & Simoncelli, 2001) means that our gain control might be cortical, or might represent the net effect of gain controls at several levels of the visual nervous system. Clearly there are many possble variations on this sort of model, and we make no claim for uniqueness; rather we have shown that a model of this general kind is capable of accounting for the variety of dynamic edge sharpening phenomena observed.

§§§§§§§§§§§§§§§§§§§§§§§§§§§§§§

Acknowledgements

This work was supported by a Wellcome Trust project grant (056093) to MAG & STH.

Figure Legends

Fig 1. A: the range of variation in luminance profiles of stimuli from square-wave to sinusoid. The solid curve is a blur profile constructed by replacing the square-wave edges with sine-wave half-periods centred on the edges. Edge blur width is defined by this half-period, in min arc. B: Example of the sigmoidal transducer function defined by equation 1. C: How a blurred grating (solid curve) is sharpened (dashed curve) by the transducer shown in (B). D: layout of the two stimulus windows on the display screen; shown to scale for an edge width of 60 min arc (spatial frequency, 0.25 c/deg).

Fig 2. Block diagram of the transducer model, with dynamic contrast gain control (Hammett et al, 2003).

Fig 3. Blur matching results for two observers (different symbols ± 1 s.e.) for flickering (A,B,C), moving (D,E,F) and flashed (G,H,I) edges. Edge widths were 15, 30, and 60 min arc, as shown for each column. For the motion graphs (D,E,F) both the speed axis (below) and the temporal frequency axis (above) are appropriately scaled. Solid curves show predictions of the gain control model using parameters given in the appendix. Experimental blur matches (and model blur codes) are expressed as percentages of the baseline match (or code). Data in G,H,I are re-plotted from Georgeson & Hammett (2002) for the same edge widths (15, 30, 60 min) as above, but in this case the gratings were pure sine-waves without the luminance plateau shown in Fig. 1A.

Fig 4. Data re-plotted from Fig. 3 A,B to compare the percentage sharpening induced by motion and by flicker at corresponding temporal frequencies for observers SB (filled symbols) and DS (open symbols). Lines of slope 1 (solid) and 0.5 (dashed) are shown.

Fig 5. Worked example of the gain control model (Fig. 2) for a 48 ms flashed grating with edge width = 30’ (period 60'). Model parameters given in Table 1. Each pane shows a space-time image of the response at a given stage (horizontal axis is time), along with graphs of spatial (X) and temporal (T) profiles taken at the positions marked by black lines in the space-time image. X-range is 240 min arc, T-range is 375 ms. Large early spike in the response R3 reflects delay in the gain control signal (where G is briefly low) but because of saturation this spike is not so prominent in the transduced signal, R4. Final coding of edge blur operates on the R4 signal, as described in the text. Final pane (right) shows the raw blur code b(t) (upper graph) and the contrast-weighted blur code b(t).w(t)/max(w) (lower graph). The final blur estimate B is the weighted average of b(t), and is compared with the baseline estimate (B_0) obtained from a 500 ms presentation. This percentage (79%) implies that 21% sharpening is predicted for this stimulus condition.

Fig 6. Similar to Fig. 5, but for 4 Hz counterphase flicker, with edge width = 30’ (period 120').

Fig 7. Similar to Fig. 6, but for 8 Hz counterphase flicker, again with edge width = 30’ (period 120').

Appendix – Model definition & parameters

The model architecture sketched in Fig. 2 was implemented in *Matlab* by a set of equations defining each linear filter and nonlinear operation. The stimulus is defined by an array of luminance values L(x,t) distributed over space (x) and time (t) sampled at intervals of 1 min arc and 2 msec respectively, with mean L_0. The input to the model was taken as the local pixel contrast C(x,t):

$$C(x,t) = \frac{L(x,t) - L_0}{L_0}.$$

Linear spatio-temporal filters f1 and f2 were formed as the separable products of spatial and temporal kernels. The temporal kernel *h* was a simple, low-pass, n-stage exponential filter (with n=3):

$$h(t;\tau) = \left(\frac{t}{\tau}\right)^n \exp\left(\frac{-t}{\tau}\right)$$

and it was normalised to have unit area:

$$h'(t;\tau) = \frac{h(t,\tau)}{\sum h(t,\tau)}.$$

The role of *f1* was essentially to transmit the image data, with slight temporal smoothing, so its spatial kernel was just a unit impulse function δ(x) that has no filtering effect, thus:

$$f1(x,t;\tau_1) = \delta(x).h'(t;\tau_1).$$

The even-symmetric spatial kernel for $f2_e$ was the second derivative g_2 of a Gaussian, scaled to have unit peak amplitude in the Fourier domain:

$$g_2(x;\sigma_2) = \left(\frac{{\sigma_2}^2 e}{2}\right) \cdot \frac{\partial^2 g(x;\sigma_2)}{\partial x^2}$$

where

$$g(x;\sigma) = \left(\frac{1}{\sigma\sqrt{2\pi}}\right) \exp\left(\frac{-x^2}{2\sigma^2}\right).$$

Multiplying the spatial and temporal kernels gave the spatio-temporal kernel:

$$f2_e(x,t;\sigma_2,\tau_2) = g_2(x;\sigma_2)h'(t;\tau_2).$$

The corresponding odd-symmetric receptive field $f2_o$ was formed by taking the Hilbert transform H{} of the spatial kernel:

$$f2_o(x,t;\sigma_2,\tau_2) = H\left\{g_2(x,\sigma_2)\right\}.h'(t;\tau_2).$$

Responses R1, R2 were computed as the convolution of the filter kernels with the input space-time image C, implemented by multiplication in the Fourier domain. Edge artefacts were avoided by ensuring that an integer number of spatial cycles was present in the image. Thus:

$$R1 = C(x,t) \otimes f1(x,t)$$
$$R2_e = C(x,t) \otimes f2_e(x,t)$$
$$R2_o = C(x,t) \otimes f2_o(x,t).$$

The energy image R2(x,t) was computed as the quadratic sum of even and odd responses, smoothed by convolution with a unit-area Gaussian of scale σ_s:

$$R2 = g(x;\sigma_s) \otimes \sqrt{R2_e^{\,2} + R2_o^{\,2}}\,.$$

Output of the gain-control signal processing is $G = a + k.R2$, and this is divided into the image data R1, to give R3 = R1/G. Finally the transducer has the form of a simple Naka-Rushton function:

$$R4 = \frac{R3}{S + |R3|}.$$

This saturates at maximum (or minimum) output values of ±1 when the magnitude of R3 (positive or negative) is large (see Fig. 1B), and it reaches half the saturated response when R3 = ±S. If S is made smaller, R4 saturates at lower input levels and so produces more distortion of the input spatial waveform. Simple substitutions yield:

$$R4 = \frac{R1}{S.(a + k.R2) + |R1|},$$

implying that distortion should increase when the energy signal R2 is attenuated at higher speeds or temporal frequencies.

Edge blur in the image R4 is evaluated moment-by-moment using the multi-scale blur-coding model outlined by Georgeson (2001) and Barbieri-Hesse & Georgeson (2002), to yield a time-varying blur code *b(t)*. Its application here is summarized by Hammett et al (2003). The final blur code B is a weighted average of the values *b(t)*, obtained using weights w(t) given by the amplitude of R1(x,t) at time t. Hence the final blur code is given by:

$$B = \frac{\sum w(t).b(t)}{\sum w(t)}.$$

Parameters for the present simulations are given in Table 1. They are consistent with those used by Hammett et al (2003) except that the time-constant τ_1 was increased from 2 to 3 ms, and τ_2 was decreased from 40 to 8 ms. The latter may appear to be a large change, but is justified because our comparison of 3 presentation modes here constrains the choice of temporal parameters more strongly than before. In particular, the flash predictions were poor with such a large τ_2. In the space domain, we suppose that the size of the spatial operators will scale with the spatial period of the grating (Table 1), to render the coding nearly scale invariant. In the previous study (Hammett et al, 2003), the spatial filter scale parameter σ_2, and energy smoothing scale σ_s , followed the same rules but were constant because the spatial period of the grating was fixed at 480 min.

Table 1 – Parameters used in the simulation

Mechanism	*Parameter*	*Value*
Filter, f1	τ_1	3 ms
Filter, f2	σ_2	(spatial period)/16
	τ_2	8 ms
Energy smoother	σ_s	(spatial period)/8
Gain constants	a	0.002
	k	3.26
Transducer	S	2
Blur coding		parameter-free

References

Anderson CH & Van Essen DC, 1987 Shifter circuits: a computational strategy for dynamic aspects of visual processing. *Proceedings of the National Academy of Science* **84** 6297-6301

Barbieri-Hesse G S A, Georgeson M A, 2002 "Template model for blur coding: the role of early nonlinearity in edge segmentation" *Perception* **31** supplement, 54

Barlow HB 1958 Temporal and spatial summation in human vision at different background intensities *Journal of Physiology* (London) **141** 337-350

Benardete E A, Kaplan E, Knight B W, 1992 "Contrast gain control in the primate retina: P cells are not X-like, some M cells are" *Visual Neuroscience* **8** 483-486

Benardete E A, Kaplan E, 1999 "The dynamics of primate M retinal ganglion cells" *Visual Neuroscience* **16** 355-368

Berry M J, Brivanlou I H, Jordan T A, Meister M, 1999 "Anticipation of moving stimuli by the retina" *Nature* **398** 334-338

Bex PJ, Edgar GK & Smith AT, 1995 Sharpening of drifting, blurred images *Vision Research* **35** 2539-2546

Burr D, 1980 "Motion smear" *Nature* **284** 164-165

Burr D C &Morgan M J, 1997 Motion deblurring in human vision *Proceedings Of the Royal Society Of London B* **264** 431-436

Chen S, Bedell HE & Ogmen H, 1995 A target in real motion appears blurred in the absence of other proximal moving targets. *Vision Research* **35** 2315-2328

Finney DJ, 1971 *Probit Analysis (*Cambridge: Cambridge University Press)

Galvin SJ, O'Shea RP, Squire AM &Hailstone DS, 1999 Sharpness overconstancy: the roles of visibility and current context *Vision Research* **39** 2649-2657

Georgeson MA, 1987 Temporal properties of spatial contrast vision. *Vision Research* **25** 765-780

Georgeson, M.A. & Hammett, S.T., 2002 "Seeing blur: 'Motion sharpening' without motion" *Proceedings of the Royal Society B* **269** 1429-1434

Georgeson M A, 2001 "Seeing edge blur: receptive fields as multi-scale neural templates" *Journal of Vision* **1** 438

Gorea A & Tyler CW 1986 New look at Bloch's law for contrast. *J. Opt. Soc. Am. A* ***3*** 52-61

Hammett S T, 1997 Motion blur and motion sharpening in the human visual system. *Vision Research* **37** 2505-2510

Hammett S T & Bex P J, 1996 Motion sharpening: evidence for the addition of high spatial frequencies to the effective neural image *Vision Research* **36** 2729-2733

Hammett ST, Georgeson MA & Gorea A, 1998 Motion blur and motion sharpening: temporal smear and local contrast non-linearity. *Vision Research* **38** 2099-2108

Hammett S T, Georgeson M A, Bedingham S, Barbieri-Hesse G S, 2003 "Motion sharpening and contrast: gain control precedes compressive non-linearity ?" *Vision Research* (in press)

Heeger D J, 1992 "Normalization of cell responses in cat striate cortex" *Visual Neuroscience* **9** 181-197

Kelly D H, 1966 "Frequency doubling in visual responses" *Journal of the Optical Society of America* **56** 1628-1633

Kelly D H, 1981 “Nonlinear visual responses to flickering sinusoidal gratings” *Journal of the Optical Society of America* **71** 1051-1055

Legge GE, 1978 Sustained and transient mechanisms in human vision: temporal and spatial properties. *Vision Research* **18** 69-81

Martin K E & Marshall JA, 1993 "Unsmearing visual motion: Development of long range horizontal intrinsic connections" in Eds SJ Hanson, JD Cowan & CL Giles *Advances in neural information processing systems*. (San Mateo, CA: Morgan Kauffman)

Pääkkönen A K, & Morgan M J, 1994 Effects of motion on blur discrimination. *J. Opt. Soc. Am. A* **11** 992-1002

Pääkkönen A K, & Morgan M J, 2001 Linear mechanisms can produce motion sharpening *Vision research* **41** 2771-2777

Ramachandran VS, Madhusudhan Rao V & Vidyasgar T R, 1974 Sharpness constancy during movement perception. *Perception* **3** 97-98

Shapley R M, Victor J D, 1978 “The effect of contrast on the transfer properties of cat retinal ganglion cells” *Journal of Physiology* **285** 275-298

Shapley R M, Victor J D, 1979 “Nonlinear spatial summation and the contrast gain control of cat retinal ganglion cells” *Journal of Physiology* **290** 141-161

Shapley R M, Victor J D, 1981 “How the contrast gain control modifies the frequency responses of cat retinal ganglion cells” *Journal of Physiology* **318** 161-179

Schwartz O, Simoncelli E P, 2001 “Natural signal statistics and sensory gain control” *Nature neuroscience* **4** 819-825

Simoncelli E P, Heeger D J, 1998 “A model of neuronal responses in visual area MT” *Vision Research* **38** 743-761

Taylor M M & Creelman C D, 1967 PEST: Efficient estimates on probability functions. *Journal of the Acoustical Society of America* ***41*** 782-787

Wilson HR 1997 A neural model of foveal light adaptation and afterimage formation *Visual Neuroscience* **14** 403-423